Resonance Analysis and Faulty Feeder Identification of High-Impedance Faults in a Resonant Grounding System

Yongduan Xue, *Member, IEEE*, Xiaoru Chen, Huamao Song, and Bingyin Xu, *Member, IEEE*

Abstract—High-impedance faults (HIF) occur frequently in resonant grounding systems and are difficult to detect. Thus, an effective HIF feeder identification technology is urgently needed. This paper establishes an HIF equivalent circuit in a resonant grounding system. The change rule of transient zero-sequence voltage, transient zero-sequence currents, and their projection components with respect to the transient zero-sequence voltage of the bus are analyzed in both underdamping and overdamping resonance conditions. Furthermore, the variation ranges of the resonant frequency, the magnitude, the attenuation factor, and other parameters are specified in detail. The magnitude and phase relationships of zero-sequence currents among the faulty feeder, healthy feeders, Petersen coil, and fault points, as well as the relationships between their projection components and quadrature components with respect to the transient zero-sequence voltage are analyzed and compared. A novel faulty feeder identification method based on a comparison of the magnitude and polarity of the transient zero-sequence current's projection component is proposed. The accuracy of the transient characteristics and the feasibility of the proposed method are verified by simulations and field data.

Index Terms—Resonant grounding system, HIF, equivalent circuit, resonance analysis, faulty feeder identification.

NOMENCLATURE

L_p Zero-sequence inductance of the Petersen coil (3 times the Petersen coil inductance).

$C_{0\Sigma}$ Sum of zero-sequence distributed capacitance to the ground of all feeders.

L Sum of the faulty feeder inductance and transformer inductance.

R Sum of faulty feeder resistance, transformer resistance and three times the fault resistance R_f.

R_f Fault resistance.

C_{0j} Zero-sequence distributed capacitance to the ground of the feeder j, $j = 1, 2, \ldots, i, \ldots, n-1, n$.

v Detuning of the Petersen coil, typically in the range of $-0.1 \le v \le 0$; in this paper, $v = -0.08$.

$u_f(t)$ Equivalent virtual voltage source; has the same magnitude and opposite phase with respect to the pre-fault phase-to-ground voltage at the fault point.

U_m Peak value of $u_f(t)$.

u_{0b} Zero-sequence voltage of the bus.

u_{0b_T} Transient component of u_{0b}.

u_{0b_PF} Power frequency component of u_{0b}.

i_{0f} Zero-sequence current of the fault point.

i_{0f_T} Transient component of i_{0f}.

i_{0f_PF} Power frequency component of i_{0f}.

i_{0Lp} Zero-sequence current of the Petersen coil.

i_{0Lp_T} Transient component of i_{0Lp}.

i_{0Lp_PF} Power frequency component of i_{0Lp}.

$i_{0Lp\_T\_P}$ Projection component of i_{0Lp_T} with respect to u_{0b_T}.

$i_{0Lp\_T\_Q}$ Quadrature component of i_{0Lp_T} with respect to u_{0b_T}.

$i_{0C0\Sigma}$ Zero-sequence ground capacitance current of the system.

i_{0C0j} Zero-sequence ground capacitance current of feeder j.

i_{0C0j_T} Transient component of i_{0C0j}.

i_{0j} Zero-sequence current of feeder j.

i_{0j_T} Transient component of i_{0j}.

i_{0j_PF} Power frequency component of i_{0j}.

$i_{0j\_T\_P}$ Projection component of i_{0j_T} with respect to u_{0b_T}.

$i_{0j\_T\_Q}$ Quadrature component of i_{0j_T} with respect to u_{0b_T}.

ξ_j Projection coefficient of feeder j.

ξ_{Lp} Projection coefficient of the Petersen coil.

θ Phase of $u_f(t)$, fault inception angle.

φ Phase of i_{0Lp}.

ω_f Transient resonant frequency in the over-damping state.

ω_0 Power frequency; in this paper, $\omega_0 = 314$ rad/ s.

d Peak value of i_{0f_T}.

I. INTRODUCTION

IN CHINA and continental Europe, resonant grounding systems exist in medium-voltage distribution networks. A single-phase earth fault does not need to be cleared immediately and can effectively improve the power supply availability. However, the fault current is typically weak and difficult to detect. Several new faulty feeder identification technologies have been developed in recent years. These technologies are based on fault transient electrical quantities and inserting resistance between neutral and the earth and effectively solve the low-impedance fault detection problem.

However, because of the natural environment, low overhead line and other factors, single-phase high-impedance faults (HIFs) frequently occur when conductors break and fall to the ground and when conductors touch tree branches [1]. HIFs account for 12% of all grounded faults in France [2]. HIF detection in a resonant grounding system is still a considerable challenge because the fault current can decrease to less than 2 A and the fault point is unstable.

Many novel approaches for the detection of HIF have been proposed since the 1970s. In a directly grounded system, the maximum HIF current is 75 A. When the conductor touches the concrete surface with rebar in a 15 kV system [3], it can be recognized as a HIF when the fault resistance is larger than 115 Ω. Many detection methods have been presented in the literature. References [4], [5] describe a apparatus that monitors and analyzes the load current to obtain an energy value and then compares the energy value with a threshold value to detect the HIF. Reference [6] monitors the energy variance of the second, fourth and sixth harmonics generated by the three-phase unbalanced current to detect the HIF. The accuracy of this method is high when the arc fault current is at least 5 A. Reference [7] uses the wavelet coefficient energy change of the distortion current to identify the HIF. Other methods use a fast Fourier transform (FFT) [8], Kalman filter [9] or wavelet transform [10]–[13] to extract the components of some special frequency band from the fault currents and voltages and then use the nonlinear distortion of the HIF to detect the fault by comparing the magnitude, phase, or energy of the special frequency band components. In a directly grounded system, the HIF detection technologies have satisfactory simulation results, and some have good practical application; thus, HIF detection technologies in a resonant grounding system can employ some of their techniques. The HIF detection methods for a resonant grounding system are less established. Reference [14] uses the phasor relationship of the three-phase current variation before and after the fault to calculate the admittance to ground; the faulty feeder has the largest admittance to ground. However, the three-phase currents are influenced by the inconsistency of the Current Transformers (CTs) of the three phases, which affects the practical application performance. Reference [15] uses the active power component of the zero-sequence power frequency current to determine the faulty feeder in the HIF. The HIF active current is small and influenced by the transmission error of CT and potential transformer (PT), which will also affect the practical application performance. References [16], [17] perform the
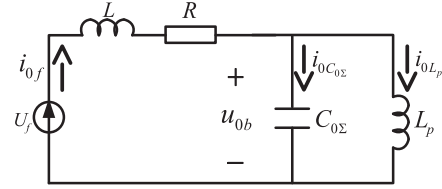

Fig. 1. Equivalent circuit of a single-phase earth fault in a resonant grounding system.

integration of the zero-sequence current of all feeders from the time when the zero-sequence voltage is zero up to the actual trigger time. The faulty feeder is the one in which the integration of the zero-sequence current is no longer proportional to the zero sequence voltage. The practical application performance is good, but the integration accumulates error easily, and the linear relation and nonlinear relation judgment are strongly influenced by the subjective factors. Thus, the algorithm must be further improved. In this paper, a novel transient approach for a resonant grounding system is proposed. The new method uses the projection of transient current with respect to transient voltage to detect the HIF.

The remainder of this paper is organized as follows. In Section II, the HIF equivalent circuit in a resonant grounding system is established. In Section III, the change rule of the zero-sequence current in each feeder and the zero-sequence voltage of the bus, together with the relationships of their transient components, in the over-damping state are analyzed. Additionally, the variation ranges of the magnitude and the attenuation factor of the transient zero-sequence current are presented. In Section IV, the resonance process and distribution of the transient current in the under-damping state are analyzed. Furthermore, the variation ranges of the frequency, magnitude and attenuation factor of the transient zero-sequence current are presented. In Section V, a novel method based on comparing the magnitude and polarity of the projection current of each feeder is proposed. In Section VI, the verification results obtained using the Alternative Transients Program (ATP), MATLAB simulation and field data are presented. Finally, conclusions are drawn in Section VII.

II. HIF EQUIVALENT CIRCUIT

Reference [18] establishes a third-order equivalent circuit of a single-phase earth fault in a resonant grounding system. The circuit, shown in Fig. 1, precisely simulates both the fault transient and power frequency electrical parameters.

The third-order differential equation is difficult to solve. Thus, the equivalent circuit should be simplified into a second-order system to obtain the analytic solutions of the electrical parameters, particularly the transient components. For a fault transient process, ω_f is generally over 1,000 rad/s when the transition resistance is low; thus,

$$R \ll |j\omega_f L| \tag{1}$$

and

$$\left|\frac{1}{j\omega_f C_{0\Sigma}}\right| \ll |j\omega_f L_p| \tag{2}$$
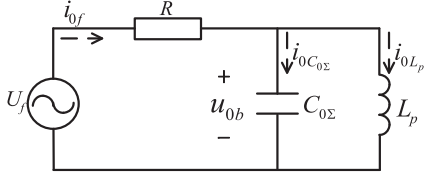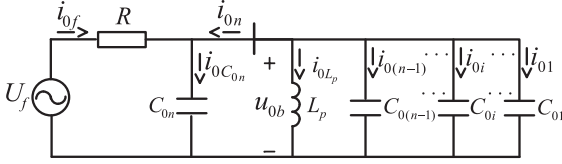
Fig. 2. Equivalent circuit of a HIF in a resonant grounding system.

Fig. 3. Equivalent HIF circuit in a resonant grounding system with n feeders.

Under these conditions, the main resonance process is the series resonance among R, L and $C_{0\Sigma}$; the effect of the Petersen coil can be ignored. A series resonance process of this type and the characteristics of transient electrical parameters are analyzed in detail in [16]–[18]. Feeder identification methods based on the transient electrical parameters of the low-impedance fault have been successfully used in the field [16]–[19].

However, when the transition resistance is high, the resonant frequency is generally less than 330 rad/s, i.e.,

$$R > 3\left|j\omega_f L\right| \tag{3}$$

or

$$\left|\frac{1}{j\omega_f C_{0\Sigma}}\right| \geq \left|j\omega_f L_p\right| \tag{4}$$

Under such circumstances, the effect of the Petersen coil increases, whereas the effect of L decreases such that it can be ignored. According to (3) and the general parameters of the distribution network (10 kV, system zero-sequence capacitance current no more than 67 A), e.g., a system zero-sequence capacitance current of 33 A, when the cable line is less than 10 km or the overhead line is less than 80 km from the fault point to the bus, the minimum value of R is approximately 60 Ω. Therefore, a HIF is known to occur when the fault resistance R_f is more than 20 Ω. An equivalent circuit of the HIF for a resonant grounding system can be obtained by combining and simplifying the aforementioned equations based on the assumptions above, as shown in Fig. 2.

A system with n feeders $(j = 1, 2, \ldots, n)$, shown in Fig. 3, can be obtained from Fig. 2 by dividing $C_{0\Sigma}$ into n branches. The faulty feeder is named feeder n. The healthy feeders are represented as $(i = 1, 2, \ldots, n - 1)$.

The following equation is established according to Fig. 3:

$$i_{0n} = i_{0C_{0n}} - i_{0f} = -\left(\sum_{i=1}^{n-1} i_{0i} + i_{0Lp}\right) \tag{5}$$

According to Figs. 2 and 3, the parallel resonance among R, L_p and $C_{0\Sigma}$ is actually the transient process of the HIF. The

differential equations for the process are established as follows:

$$\begin{cases} u_f(t) = R\left(C_{0\Sigma}\dfrac{du_{0b}}{dt} + i_{oL_P}\right) + L_P\dfrac{di_{0L_P}}{dt} \\[2mm] u_{0b} = L_P\dfrac{di_{0L_P}}{dt} \\[2mm] u_f(t) = U_m\sin(\omega_0 t + \theta) \end{cases} \tag{6}$$

As a second-order non-homogeneous linear equation, the characteristic roots are

$$p_1 = -\frac{1}{2RC_{0\Sigma}} - \sqrt{\left(\frac{1}{2RC_{0\Sigma}}\right)^2 - \frac{1}{L_P C_{0\Sigma}}}$$

$$p_2 = -\frac{1}{2RC_{0\Sigma}} + \sqrt{\left(\frac{1}{2RC_{0\Sigma}}\right)^2 - \frac{1}{L_P C_{0\Sigma}}} \tag{7}$$

This paper mainly focuses on the resonance processes in the over-damping and under-damping states.

III. RESONANCE PROCESS AND DISTRIBUTION OF TRANSIENT CURRENT IN THE OVER-DAMPING STATE

A. Resonance Process in the Over-Damping State

The resonance process is in an over-damping state when R satisfies the following equation:

$$3\left|j\omega_0 L\right| < R < \frac{1}{2}\sqrt{\frac{L_P}{C_{0\Sigma}}} = \frac{1}{2\omega_0 C_{0\Sigma}\sqrt{1-\nu}} \tag{8}$$

A zero-sequence current through a Petersen coil can be expressed as

$$\begin{aligned} i_{0L_P} &= i_{0L_P\_T} + i_{0L_P\_PF} \\ i_{0L_P\_T} &= A_1 e^{p_1 t} + A_2 e^{p_2 t} \\ i_{0L_P\_PF} &= B\sin(\omega_0 t + \varphi) \end{aligned} \tag{9}$$

A zero-sequence current at the fault point can be expressed as

$$\begin{aligned} i_{0f} &= i_{0L_P} + i_{0C_{0\Sigma}} = i_{0f\_T} + i_{0f\_PF} \\ i_{0f\_T} &= -\frac{L_P p_1 A_1}{R}e^{p_1 t} - \frac{L_P p_2 A_2}{R}e^{p_2 t} \\ i_{0f\_PF} &= (1 - \omega_0^2 L_P C_{0\Sigma})B\sin(\omega_0 t + \varphi) \end{aligned} \tag{10}$$

where

$$B = \frac{U_m}{|Z|}\cdot\frac{1}{1 - \omega_0{}^2 L_P C_{0\Sigma}} = \frac{U_m}{|Z|}\cdot\frac{1-\nu}{-\nu}$$

$$Z = R + \frac{j\omega_0 L_P}{1 - \omega_0{}^2 L_P C_{0\Sigma}} = R + \frac{1}{jv\omega_0 C_{0\Sigma}}$$

$$A_1 = \frac{\omega_0 B\cos\varphi - p_2 B\sin\varphi}{p_2 - p_1}$$

$$A_2 = -\frac{\omega_0 B\cos\varphi - p_1 B\sin\varphi}{p_2 - p_1}$$

$$\varphi = \theta - \arctan\frac{\omega_0 L_p}{R(1 - \omega_0{}^2 L_P C_{0\Sigma})} \tag{11}$$

As shown in (9) and (10), both i_{0f} and i_{0Lp} are composed of a power frequency component and transient components (two independent decaying direct current components). Because the initial values of two decaying direct current components cannot be 0 at the same time, the attenuation factors are unequal and the transient components always exist.

The initial value of the transient component of i_{0Lp} can be expressed as

$$- B \sin \varphi \qquad (12)$$

Thus, the initial value reaches the maximum and is equal to the peak value of the power frequency zero-sequence current of the Petersen coil when θ is approximately 0° or 180°.

The initial value of the transient component of i_{0f} can be expressed as

$$\frac{L_P}{R} \omega_0 B \cos \varphi \qquad (13)$$

Thus, the initial value reaches the maximum when θ is approximately 90° or 270°. According to (8), the maximum initial value can be calculated as follows:

$$\frac{L_P}{R} \omega_0 B > \frac{2B}{\sqrt{1-\nu}} \approx 2B \qquad (14)$$

The maximum initial value is larger than the peak value of the system zero-sequence capacitance current and also considerably larger than the amplitude of the power frequency zero-sequence current at the fault point. When $A_1 A_2 < 0$, the initial value of the transient current is small; however, another maximum value of the transient component would appear because of the difference of the two attenuation factors. It can be proven that the maximum value of the transient component is larger than that of the power frequency component. Additionally, this maximum typically varies from tens of amperes to hundreds of amperes.

Attenuation factors reflect the duration of the transient process: fault identification is easier when the attenuation of the transient process is slower. The characteristic roots p_1 and p_2 satisfy the following conditions:

$$-\frac{\omega_0}{0.03|X_L|} - \sqrt{\left(\frac{\omega_0}{0.03|X_L|}\right)^2 - \frac{1}{\omega_0{}^2(1-\nu)}} < p_1$$
$$< \omega_0\sqrt{1-\nu} \quad \omega_0\sqrt{1-\nu} < p_2 < -\frac{\omega_0}{0.03|X_L|}$$
$$+ \sqrt{\left(\frac{\omega_0}{0.03|X_L|}\right)^2 - \frac{1}{\omega_0{}^2(1-\nu)}} \qquad (15)$$

p_1 and p_2 become closer to each other as R increases. For the aforementioned system with 33 A system zero-sequence capacitance current, the characteristic roots are typically in the range of $-1681.1 < p_1 < -326.3 < p_2 < -63.3$, indicating that the duration of the transient component varies from several milliseconds to tens of milliseconds.

In conclusion, the magnitude and duration of the fault current's transient component in the over-damping state can satisfy the conditions required for identification.

B. Distribution of the Transient Current in the Over-Damping State

The zero-sequence voltage of the bus can be expressed as

$$
\begin{aligned}
u_{0b} &= u_{0b\_T} + u_{0b\_PF} \\
u_{0b\_T} &= L_P p_1 A_1 e^{p_1 t} + L_P p_2 A_2 e^{p_2 t} \\
u_{0b\_PF} &= \omega_0 L_P B \cos(\omega_0 t + \varphi)
\end{aligned} \qquad (16)
$$

The zero-sequence current of healthy feeders, which is equal to its zero-sequence capacitance ground current, can be expressed as

$$
\begin{aligned}
i_{0i} &= i_{0i\_T} + i_{0i\_PF} \\
i_{0i\_T} &= L_P C_{0i}(A_1 p_1{}^2 e^{p_1 t} + A_2 p_2{}^2 e^{p_2 t}) \\
i_{0i\_PF} &= -\omega_0{}^2 L_P C_{0i} B \sin(\omega_0 t + \varphi)
\end{aligned} \qquad (17)
$$

The zero-sequence current of a faulty feeder can be expressed as

$$
\begin{aligned}
i_{0n} &= i_{0n\_T} + i_{0n\_PF} \\
i_{0n\_T} &= \left(\frac{L_P p_1 A_1}{R} + L_P C_{0n} A_1 p_1{}^2\right) e^{p_1 t} \\
&\quad + \left(\frac{L_P p_2 A_2}{R} + L_P C_{0n} A_2 p_2{}^2\right) e^{p_2 t} \\
i_{0n\_PF} &= (\omega_0^2 L_P (C_{0\Sigma} - C_{0n}) - 1) B \sin(\omega_0 t + \varphi)
\end{aligned} \qquad (18)
$$

i_{0j} is composed of the power frequency component i_{0j_PF} and transient component i_{0j_T}. i_{0j_T} is the sum of two decaying direct current components.

In a healthy feeder, the power frequency component of i_{0i} leads that of u_{0b} by nearly 90°, and the magnitude is directly proportional to C_{0i}. However, for the faulty feeder, the power frequency component of i_{0n} shares the same phase with i_{0i}, and the magnitude may be larger or smaller than that of the healthy feeder. Therefore, the HIF feeder cannot be identified by the power frequency current.

For the healthy feeders, the polarities of their transient currents i_{0i_T} are the same, and their magnitudes are directly proportional to C_{0i}. The faulty feeder transient current i_{0n_T} comprises two parts. One part is i_{0f_T} and is directly proportional to u_{0b_T} (the ratio coefficient is $1/R$). The other part is i_{0C0n_T} and has the same characteristics as i_{0i_T}. Therefore, the magnitude of the transient current of the faulty feeder is not always the largest, and its polarity is neither the same nor the reverse as those of the healthy feeders. Thus, it is difficult to detect the HIF directly with the transient current.

IV. RESONANCE PROCESS AND DISTRIBUTION OF THE TRANSIENT CURRENT IN THE UNDER-DAMPING STATE

A. Resonance Process in the Under-Damping State

When R is in the following range:

$$R > \frac{1}{2}\sqrt{\frac{L_P}{C_{0\Sigma}}} \qquad (19)$$

the system is in an under-damping state. An under-damping state is the main state of an HIF.

The zero-sequence current through a Petersen coil can be expressed as

$$i_{0LP} = i_{0LP\_T} + i_{0LP\_PF}$$
$$i_{0LP\_T} = e^{-\delta t}(A_3 \cos(\omega_f t) + A_4 \sin(\omega_f t))$$
$$i_{0LP\_PF} = B \sin(\omega_0 t + \varphi) \tag{20}$$

The zero-sequence current at the fault point can be expressed as

$$i_{0f} = i_{0LP} + i_{0C_{0\Sigma}} = i_{0f\_T} + i_{0f\_PF}$$
$$i_{0f\_T} = -\frac{L_P(A_4\omega_f - \delta A_3)}{R}e^{-\delta t}\cos(\omega_f t)$$
$$\quad -\frac{L_P(-A_3\omega_f - \delta A_4)}{R}e^{-\delta t}\sin(\omega_f t)$$
$$i_{0f\_PF} = (1 - \omega_0^2 L_P C_{0\Sigma})B\sin(\omega_0 t + \varphi) \tag{21}$$

where

$$A_3 = -B\sin\varphi; A_4 = \frac{-\delta B\sin\varphi - \omega_0 B\cos\varphi}{\omega_f} \tag{22}$$

Both i_{0f} and i_{0Lp} comprise a power frequency component and transient component (an attenuation sine component). δ and ω_f are as follows:

$$\delta = \frac{1}{2RC_{0\Sigma}} \tag{23}$$

$$\omega_f = \sqrt{\frac{1}{L_P C_{0\Sigma}} - \left(\frac{1}{2RC_{0\Sigma}}\right)^2} = \sqrt{\omega_0^2(1-\nu) - \delta^2} \tag{24}$$

According to (24), ω_f increases with increasing $C_{0\Sigma}$ or R. That is, for a certain system, the resonant frequency increases monotonously from 0 along with increasing R. The upper limit is

$$\omega_{f\cdot\max} = \omega_0\sqrt{1-\nu} \approx 326.32 \text{ rad/s} \tag{25}$$

corresponding to a frequency of 51.96 Hz. The maximum frequency is slightly higher than the power frequency. An obvious beat frequency phenomenon would be observed when $\omega_f \approx \omega_0$.

From (23), δ is inversely proportional to $C_{0\Sigma}$ or R. For the same R, the $C_{0\Sigma}$ of the cable line system is typically larger than that of the overhead line system; thus, the attenuation speed of the cable line system is slower than that of the overhead line system. However, for a certain system, a slower attenuation speed corresponds to a larger R. The maximum value of the attenuation factor is

$$\delta = \frac{1}{2RC_{0\Sigma}} < \omega_0\sqrt{1-\nu} = 326.32\frac{1}{s} \tag{26}$$

Although the theoretical minimum value of δ is 0, the practical minimum value is sufficiently large for fault detection. Assume that the transition resistance is 10 kΩ and the system zero-sequence capacitance current is 67 A; then, the attenuation factor δ will be 1.57. The time constant of the transient process in the under-damping state generally varies from 0.003 s to 0.6 s.
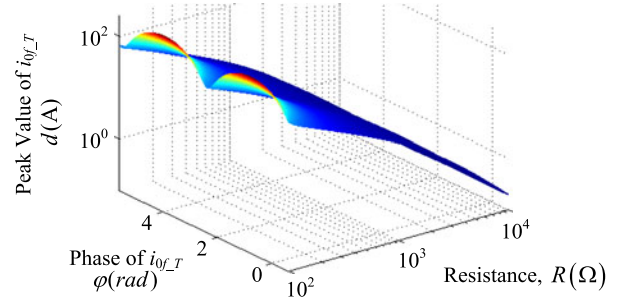

Fig. 4. Change rule of the magnitude d of i_{0f_T} with a phase angle φ and resistance R.

According to (21), the peak value of the transient component of the fault point current can be expressed as

$$d = \frac{BL_P}{R\omega_f}$$
$$\sqrt{\omega_0^4(1-\nu)^2\sin^2\varphi + \omega_0^4(1-\nu)\cos^2\varphi + \delta\omega_0^3(1-\nu)\sin 2\varphi} \tag{27}$$

Assuming that $1 - v \approx 1$, we also obtain

$$B = U_m\frac{\omega_0 C_{0\Sigma}}{\sqrt{1 + \nu^2\omega_0^2 C_{0\Sigma}^2 R^2}} \tag{28}$$

Thus, (27) can be simplified as

$$d = \frac{U_m}{R\omega_f}\frac{\sqrt{\omega_0^2 + \delta\omega_0\sin 2\varphi}}{\sqrt{1 + \nu^2\omega_0^2 C_{0\Sigma}^2 R^2}} \tag{29}$$

The magnitude of the transient component decreases with increasing R. However, the effect of φ repeats itself after half a cycle. The effect is more obvious for a lower R. The effect can be ignored when R is sufficiently high. The variation law of d with R and φ is shown in Fig. 4.

Assuming that

$$R = -\frac{1}{\nu\omega_0 C_{0\Sigma}} \tag{30}$$

then, from (24), $\omega_f \approx \omega_0$, (27) can be simplified as follows:

$$d = \frac{U_m}{\sqrt{2}R} = -\frac{U_m}{\sqrt{2}}\nu\omega_0 C_{0\Sigma} \tag{31}$$

In conclusion, for a certain system, the transient frequency becomes closer to the power frequency with increasing R. Furthermore, d becomes smaller, and the duration of the transient process becomes longer. These trends meet the conditions for fault detection requirements.

B. Distribution of the Transient Current in the Under-Damping State

The zero-sequence voltage of the bus can be expressed as

$$u_{0b} = u_{0b\_T} + u_{0b\_PF}$$
$$u_{0b\_T} = L_P(-A_3\omega_f - \delta A_4)e^{-\delta t}\sin(\omega_f t)$$
$$\quad + L_P(A_4\omega_f - \delta A_3)e^{-\delta t}\cos(\omega_f t)$$
$$u_{0b\_PF} = \omega_0 L_P B\cos(\omega_0 t + \varphi) \tag{32}$$

Similar to the over-damping state, the zero-sequence current of healthy feeders, which is equal to its zero-sequence capacitance ground current, can be expressed as

$$i_{0i} = i_{0i\_T} + i_{0i\_PF}$$

$$i_{0i\_T} = L_P C_{0i}(\delta^2 A_3 - A_3 \omega_f{}^2 - 2\delta A_4 \omega_f)e^{-\delta t}\cos(\omega_f t)$$
$$+ L_P C_{0i}(\delta^2 A_4 - A_4 \omega_f{}^2 + 2\delta A_3 \omega_f)e^{-\delta t}\sin(\omega_f t)$$

$$i_{0i\_PF} = -L_P C_{0i}\omega_0{}^2 B \sin(\omega_0 t + \varphi) \qquad (33)$$

The zero-sequence current of the faulty feeder can be expressed as

$$i_{0n} = i_{0n\_T} + i_{0n\_PF}$$

$$i_{0n\_T} = -(A_3 + L_P(C_{0\Sigma} - C_{0n})(A_3\delta^2 - A_3\omega_f{}^2$$
$$- 2A_4\omega_f\delta))e^{-\delta t}\cos(\omega_f t)$$
$$- (A_4 + L_P(C_{0\Sigma} - C_{0n})(A_4\delta^2 - A_4\omega_f{}^2$$
$$+ 2A_3\omega_f\delta))e^{-\delta t}\sin(\omega_f t)$$

$$i_{0n\_PF} = (\omega_0{}^2 L_P(C_{0\Sigma} - C_{0n}) - 1)B\sin(\omega_0 t + \varphi) \quad (34)$$

i_{0j} is composed of a power frequency component and transient component (decaying sine component i_{0j_T}), in which the characteristic of the power frequency component is the same as that in the over-damping state. i_{0i_T} leads u_{0b_T} by nearly 90°, and the magnitude is directly proportional to C_{0i}. i_{0n_T} consists of i_{0f_T} and i_{0C0n_T}, whose characteristics are also the same as those in the over-damping state.

V. HIF FEEDER IDENTIFICATION BASED ON TRANSIENT ZERO-SEQUENCE CURRENT PROJECTION

A. Principle of Transient Zero-sequence Current Projection-Based Feeder Identification

For both the over-damping and under-damping states, the projections of i_{0j_T} and i_{0Lp_T} with respect to u_{0b_T} are $i_{0j\_T\_P}$ and $i_{0Lp\_T\_P}$, respectively, which are the product of the projection coefficient (ξ_j, ξ_{Lp}) and u_{0b_T}. When in the over-damping state, the projection coefficients can be written as

$$\xi_i = \frac{\langle i_{0i\_T}, u_{0b\_T}\rangle}{||u_{0b\_T}||^2} = -\frac{1}{2}\frac{L_P{}^2 C_{0i}(A_1 p_1 + A_2 p_2)^2}{||u_{0b\_T}||^2} < 0 \quad (35)$$

$$\xi_{L_p} = \frac{\langle i_{0Lp\_T}, u_{0b\_T}\rangle}{||u_{0b\_T}||^2} = -\frac{1}{2}\frac{L_p(A_1 + A_2)^2}{||u_{0b\_T}||^2} < 0 \quad (36)$$

$$\xi_n = \frac{1}{R} + \frac{\langle i_{C_{0n}\_T}, u_{0b\_T}\rangle}{||u_{0b\_T}||^2}$$
$$= \frac{1}{R} + \frac{-\frac{1}{2}L_p{}^2 C_{0n}(A_1 p_1 + A_2 p_2)^2}{||u_{0b\_T}||^2}$$
$$= \frac{L_p{}^2(A_1 + A_2)^2 + L_p{}^2(C_{0\Sigma} - C_{0n})(A_1 p_1 + A_2 p_2)^2}{2||u_{0b\_T}||^2}$$
$$> 0 \qquad (37)$$

Specifically, the projection coefficients ξ_i and ξ_{Lp} are negative when ξ_n is positive. The same characteristics occur in the
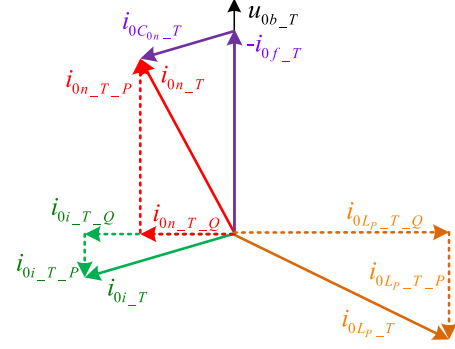

Fig. 5.   Relationship between each component in the inner product space.

under-damping state. We can also obtain the following relationship:

$$i_{0n\_T\_P} = -\left(\sum_{i=1}^{n-1} i_{0i\_T\_P} + i_{0L_P\_T\_P}\right) \qquad (38)$$

$i_{0n\_T\_P}$ has reverse polarity with $i_{0i\_T\_P}$ and $i_{0Lp\_T\_P}$, and the magnitude of $i_{0n\_T\_P}$ is always larger than those of $i_{0i\_T\_P}$ and $i_{0Lp\_T\_P}$ and can be used to identify the faulty feeder.

Apart from $i_{0j\_T\_P}$, the remaining current component of each feeder's transient current has the same polarity and is orthogonal to u_{0b_T}, which is recognized as a quadrature component. $i_{0j\_T\_Q}$ has the same polarity, and the magnitude ratio of $i_{0j\_T\_Q}$ is equal to the ratio of the capacitance to the ground of every feeder. The remaining current component of the Petersen coil is also orthogonal to u_{0b_T}. The relationship between $i_{0j\_T\_Q}$ and $i_{0Lp\_T\_Q}$ is given by the following equation:

$$i_{0L_P\_T\_Q} = -\sum_{j=1}^{n} i_{0j\_T\_Q} \qquad (39)$$

According to (39), $i_{0j\_T\_Q}$ has reverse polarity with $i_{0Lp\_T\_Q}$, and the magnitude of $i_{0j\_T\_Q}$ is always smaller than that of $i_{0Lp\_T\_Q}$.

Fig. 5 shows the relationship among i_{0f_T}, i_{0n_T}, i_{0i_T}, i_{0Lp_T}, $i_{0n\_T\_P}$, $i_{0i\_T\_P}$, $i_{0Lp\_T\_P}$, $i_{0n\_T\_Q}$, $i_{0i\_T\_Q}$, $i_{0Lp\_T\_Q}$, and u_{0b_T} in the inner product space. All these components are in the same two-dimensional plane.

B. Assessment of the Faulty Feeder Identification Algorithm

1) This method provides an effective HIF identification for a single-phase earth fault in a resonant grounding system. It improves the transient analysis and faulty feeder identification technology in a non-solidly grounding system.
2) Compared with [16], [17], the new HIF identification method has a more rigorous criterion: no accumulative error and better anti-interference performance.
3) Compared with the methods based on inserting resistance between neutral and earth, the new method does not have to install additional devices and has considerably better safety performance.
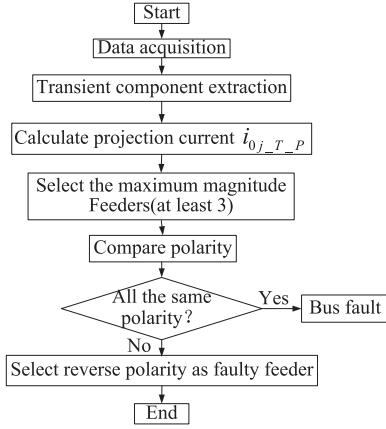4) Compared with [14], [15], the new method is less affected by PT and CT errors.

Fig. 6.   Algorithm flowchart for faulty feeder identification.

5) The new method is not affected by the line type, fault resistance, fault inception angle or fault location. It is based on the fault characteristics derived through detailed equivalent circuit analysis.

6) The new method operates according to the zero-sequence voltage which is less influenced by the switching transients. So the probability of the false detection during normal operation can be reduced greatly.

7) The new methods cannot be used for the only one feeder or two feeders circuit case. This is a typical problem for methods based on the current amplitude and polarity in faulty feeder identification.

C. Faulty Feeder Identification Criteria Based on Transient Zero-Sequence Current Projection

$i_{0j\_T\_P}$ can be calculated using the following equation:

$$i_{0j\_T\_P} = \frac{\langle i_{0j\_T}, u_{0b\_T} \rangle}{||u_{0b\_T}||^2} u_{0b\_T}, j = 1, 2, ..., n \qquad (40)$$

According to the analysis in Section V-A, the faulty feeder can be identified by comparing the magnitude and polarity of $i_{0j\_T\_P}$.

Criterion: Select at least three feeders with the highest $i_{0j\_T\_P}$ magnitudes. The feeder with the reverse polarity of the transient zero-sequence current projection among them is the faulty feeder. If the polarities of all the projections are the same, it is a bus fault.

This criterion can overcome the effect of feeders with weak current and may produce incorrect polarity calculations.

The implementation of the criterion is shown in Fig. 6.

VI. SIMULATION AND VERIFICATION

A. Simulation Models

The distributed parameter-based ATP simulation model for a typical 110 kV/10 kV distribution system is shown in Fig. 7. For a Petersen coil grounding network, the system is set to be over-compensated, with 108% compensation. The network comprises three mixed feeders with overhead lines and cables
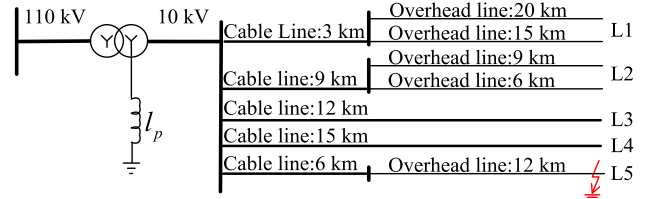

Fig. 7.   Simulation model of a resonant grounding system.

TABLE I
LINE PARAMETERS OF THE MODEL

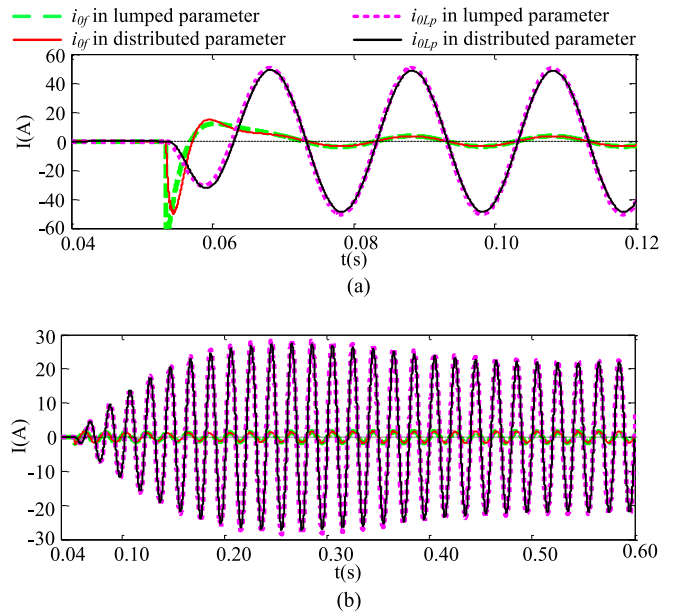| Parameters | Resistance (Ω/km) | | Inductance (mH/km) | | Capacitance (μF/km) | |
	R+	R0	L+	L0	C+	C0
Overhead Line	0.17	0.32	1.017	3.56	0.115	0.0062
Cable Line	0.27	2.7	0.255	1.109	0.376	0.276

Fig. 8.   Currents of the fault point and Petersen coil in different resonance states: (a) Zero-sequence current of fault point and Petersen coil in over-damping state. (b) Zero-sequence current of the fault point and Petersen coil in the under-damping state.

(feeders 1, 2 and 5) together with two cable feeders (feeders 3 and 4). A HIF occurs in phase A of feeder 5.

The line parameters are listed in Table I.

B. Verification of the HIF Equivalent Circuit

According to the simulation model in Fig. 7, a fault was applied at feeder 5's terminal with a fault inception angle of 90°. The equivalent circuit shown in Fig. 2 is the basis of the analysis and calculation in this paper. The simulations of the equivalent circuit in Fig. 2 (corresponding to the system in Fig. 7) have also been performed such that the error of the two models can be compared. The waveforms of i_{0j} and i_{0Lp} in the distributed parameter model are shown in Fig. 8. The waveforms in the

TABLE II
PARAMETER VERIFICATION IN THE OVER-DAMPING STATE

Transient Zero-sequence Current at the Fault Point	The Parameters of i_{0f_T}			
	A_1 (A)	A_2 (A)	p_1 (1/s)	p_2 (1/s)
Distributed Parameter Model	33.02	−33.95	−550.99	−193.05
Lumped Parameter Model	33.24	−34.49	−551.28	−193.18

TABLE III
PARAMETER VERIFICATION IN THE UNDER-DAMPING STATE

Transient Zero-sequence Current at the Fault Point	The Parameters of i_{0f_T}			
	d (A)	ω_f (rad/s)	δ (1/s)	φ (°)
Distributed Parameter Model	1.97	325.98	8.56	55.13
Lumped Parameter Model	1.95	326.20	8.68	55.38

lumped parameter equivalent circuit in Fig. 2 (corresponding to the system in Fig. 7) are also shown in Fig. 8. The system is in the over-damping state when R_f is 26 Ω in Fig. 8(a), and the system is in the under-damping state when R_f is 1,500 Ω in Fig. 8(b).

The parameters of i_{0f_T} in a distributed parameter model are extracted through the Prony algorithm [20]. The parameters of i_{0f_T} in the lumped parameter model are calculated via (7), (11), (23), (24), (27). The parameters in the over-damping and under-damping states are shown in Tables II and III, respectively.

Fig. 8 illustrates that the over-damping state has a larger transient current peak value and faster attenuation speed. Furthermore, in the under-damping state, a clear beat frequency phenomenon appears as the resonance frequency becomes close to the power frequency.

All the parameters—the magnitude and attenuation factor of a decaying direct current component in the over-damping state, as well as the frequency, magnitude, attenuation factor and phase of the transient current in the under-damping state illustrate that the lumped parameter equivalent circuit in Fig. 2 can be used to simulate a HIF. Therefore, the calculation and analysis of transient electrical parameters based on the equivalent circuit are trustworthy.

C. Verification of the Faulty Feeder Identification Method

The waveforms of u_{0b}, u_{0b_T}, i_{0j}, i_{0j_T} and $i_{0j\_T\_P}$ in the over-damping state ($R_f = 26$ Ω) and under-damping state ($R_f = 1500$ Ω) in a distributed parameter model are shown in Figs. 9 and 10, respectively, and feeder 5 is the faulty feeder. To make the graphics more intuitive, only the typical waveforms of three feeders (faulty feeder and two healthy feeders) are drawn; the other two healthy feeders are proportional to feeders 1 and 2.

The projection current into the healthy feeders is amplified in order to make the reverse polarity of the currents clear in Fig. 10(c).
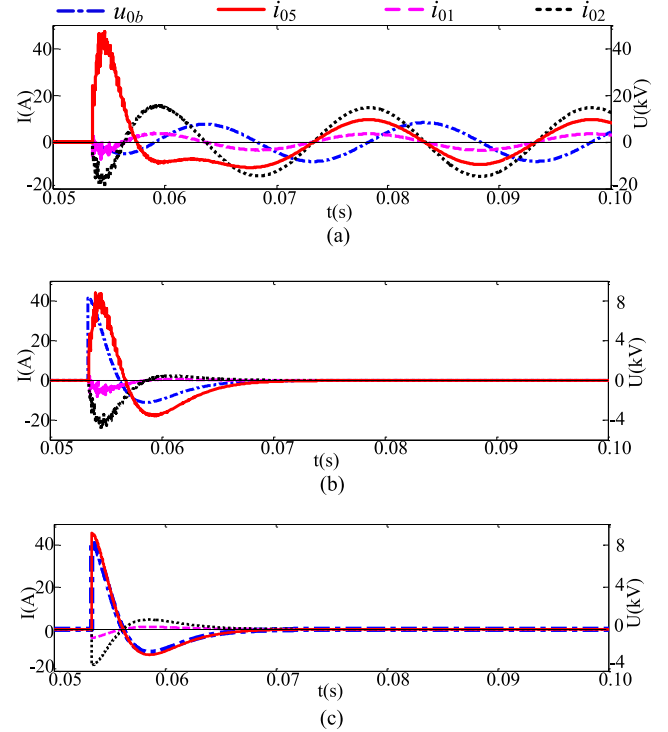

Fig. 9. Waveforms of zero-sequence current of each feeder, bus voltage and their different components in the over-damping state: (a) Zero-sequence component. (b) Transient component. (c) Projection component.

Table IV shows the projection coefficients of the transient current with respect to the bus transient voltage for all feeders in Fig. 7.

Extensive simulations have been performed in different systems, parameters, fault inception angles, transition resistances and fault locations; all conclusions are correct. In all cases, the faulty feeder has the maximum magnitude and reverse polarity of the current projection component. Thus, the faulty feeder can be accurately identified.

D. Verification of the Field Data

To verify the reliability of the method, we selected groups of field data, e.g., a group of field data from Zhoubang substation, Qingpu district, Shanghai, China in 2015. The system is 35/10 kV and the fault bus has 8 feeders. Fig. 11 shows the waveforms of u_{0b}, u_{0b_T}, i_{0j}, i_{0j_T} and $i_{0j\_T\_P}$ in the under-damping state. Feeder 'Zhou24' is the faulty feeder, and feeders 'Zhou 22' and 'Zhou 28' are healthy feeders with the highest relative current magnitudes. The projection current into the healthy feeders is amplified in order to make the reverse polarity of the currents clear in Fig. 11(c).

E. Summary of the Simulation and Field Data Verification

The waveforms in the over-damping state shown in Fig. 9 illustrate that i_{0j} and u_{0b} are the sum of two decaying direct current components and the power frequency component. For the under-damping state, i_{0j} and u_{0b} are the sum of the decaying sine component and power frequency component,
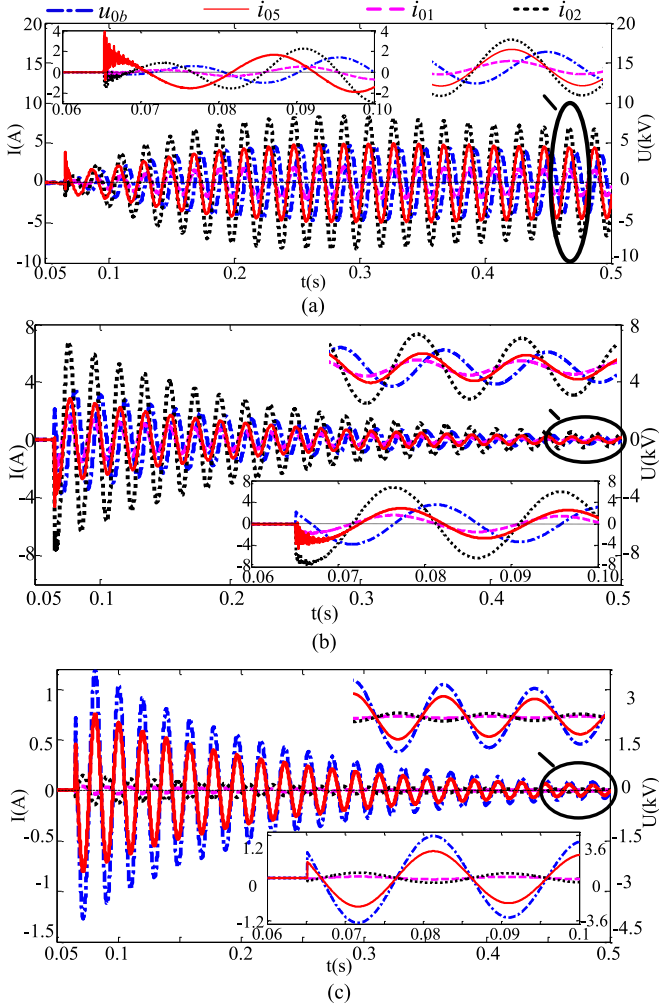
Fig. 10. Waveforms of zero-sequence current of each feeder, bus voltage and their different components in the under-damping state: (a) Zero-sequence component. (b) Transient component. (c) Projection component.

TABLE IV
SIMULATION RESULTS

Projection coefficient				Fault Inception Angle, θ				
				0	$\pi/4$	$\pi/2$	$3\pi/4$	Π
R	Over-damping cases	26 Ω	i_{01_T}	−8.7e−05	−3.5e−01	−6.7e−01	−3.2e−01	−8.7e−05
			i_{02_T}	−3.8e−03	−8.6e−01	−1.7e−00	−7.9e−01	−3.8e−03
			i_{03_T}	−6.4e−03	−1.1e−00	−2.1e−00	−1.0e−00	−6.4e−03
			i_{04_T}	−1.4e−02	−1.4e−00	−2.6e−00	−1.2e−00	−1.4e−02
			i_{05_T}	9.0e−00	8.0e−00	7.1e−00	8.1e−00	9.0e−00
	Under-damping cases	100 Ω	i_{01_T}	−3.5e−04	−1.4e−01	−2.5e−01	−1.1e−01	−3.5e−04
			i_{02_T}	−2.4e−03	−3.4e−01	−6.2e−01	−2.7e−01	−2.4e−03
			i_{03_T}	−6.3e−03	−4.3e−01	−8.0e−01	−3.5e−01	−6.3e−03
			i_{04_T}	−1.4e−02	−5.3e−01	−9.9e−01	−4.3e−01	−1.4e−02
			i_{05_T}	3.3e−00	2.9e−00	2.7e−00	3.0e−00	3.3e−00
		500 Ω	i_{01_T}	−2.4e−03	−3.9e−02	−5.1e−02	−1.4e−02	−2.4e−03
			i_{02_T}	−2.4e−03	−9.2e−02	−1.2e−01	−3.2e−02	−2.4e−03
			i_{03_T}	−2.4e−04	−1.2e−01	−1.5e−01	−3.8e−02	−2.4e−04
			i_{04_T}	−6.6e−03	−1.4e−01	−1.8e−01	−4.1e−02	−6.6e−03
			i_{05_T}	6.6e−01	5.8e−01	5.5e−01	6.3e−01	6.6e−01
		1000 Ω	i_{01_T}	−4.2e−03	−2.4e−02	−2.3e−02	−3.2e−03	−4.2e−03
			i_{02_T}	−7.0e−03	−5.7e−02	−5.5e−02	−4.3e−03	−7.0e−03
			i_{03_T}	−5.6e−03	−7.0e−02	−6.7e−02	−2.3e−03	−5.6e−03
			i_{04_T}	−5.8e−04	−8.1e−02	−7.7e−02	−3.5e−03	−5.8e−04
			i_{05_T}	−3.3e−01	2.8e−01	2.8e−01	3.3e−01	3.3e−01
		1500 Ω	i_{01_T}	−5.3e−03	−1.9e−02	−1.4e−02	−5.4e−04	−5.3e−03
			i_{02_T}	−9.5e−03	−4.3e−02	−3.1e−02	−2.1e−03	−9.5e−03
			i_{03_T}	−8.9e−03	−5.2e−02	−3.6e−02	−6.2e−03	−8.9e−03
			i_{04_T}	−4.7e−03	−5.8e−02	−3.8e−02	−1.4e−02	−4.7e−03
			i_{05_T}	2.1e−01	1.8e−01	1.9e−01	2.2e−01	2.1e−01
		2000 Ω	i_{01_T}	−5.7e−03	−1.5e−02	−9.0e−03	−1.7e−04	−5.7e−03
			i_{02_T}	−1.1e−02	−3.4e−02	−1.9e−02	−4.0e−03	−1.1e−02
			i_{03_T}	−1.0e−02	−4.0e−02	−2.0e−02	−8.6e−03	−1.0e−02
			i_{04_T}	−6.6e−03	−4.4e−02	−1.9e−02	−1.7e−02	−6.6e−03
			i_{05_T}	1.6e−01	1.4e−01	1.5e−01	1.7e−01	1.6e−01
		2500 Ω	i_{01_T}	−5.9e−03	−1.3e−02	−6.3e−03	−3.2e−04	−5.9e−03
			i_{02_T}	−1.1e−02	−2.8e−02	−1.2e−02	−4.4e−03	−1.1e−02
			i_{03_T}	−1.1e−02	−3.2e−02	−1.2e−02	−9.1e−03	−1.1e−02
			i_{04_T}	−7.2e−03	−3.4e−02	−8.5e−03	−1.8e−02	−7.2e−03
			i_{05_T}	−1.2e−01	1.1e−01	1.3e−01	1.3e−01	1.2e−01
		3000 Ω	i_{01_T}	−5.9e−03	−1.1e−02	−4.6e−03	−2.9e−04	−5.9e−03
			i_{02_T}	−1.1e−02	−2.4e−02	−7.7e−03	−4.3e−03	−1.1e−02
			i_{03_T}	−1.1e−02	−2.7e−02	−6.5e−03	−9.0e−03	−1.1e−02
			i_{04_T}	−7.1e−03	−2.7e−02	−1.7e−03	−1.8e−02	−7.1e−03
			i_{05_T}	1.0e−01	8.9e−02	1.0e−01	1.1e−01	1.0e−01

the waveforms of which are shown in Figs. 10 and 11, respectively.

The steady-state power frequency zero-sequence current of the faulty feeder leads the zero-sequence voltage by nearly 90° in both the over-damping and under-damping states. Its phase is the same as those of the healthy feeders. Additionally, the magnitude is not the maximum. Therefore, no clear fault characteristics can be observed. In the over-damping state, the magnitude of i_{0n_T} is larger than that of i_{0i_T}, while their polarities are not completely reversed. In the under-damping state, the magnitude of i_{0n_T} is not the maximum, and the phase difference with respect to the healthy feeders, i_{0i_T}, varies with R. Thus, no clear fault characteristic is observed in i_{0j_T},.

As shown in Figs. 9(c), 10(c), and 11(c), in both the over-damping and under-damping states, the magnitudes of $i_{0i\_T\_P}$ are considerably smaller than those of $i_{0n\_T\_P}$ and have completely reversed polarity, a clear fault characteristic. This conclusion is the same as that obtained in the theoretical analysis in Section V.

VII. CONCLUSION

For a resonant grounding system, the transient process of a HIF is the parallel resonance between the system capacitance to ground and the Petersen coil. The parallel resonance can be divided into the over-damping and under-damping states based on the variations of the fault resistance. In the over-damping state, the transient zero-sequence current is composed of two decaying direct current components. The under-damping state consists only of one decaying sine component with a resonant frequency that varies from 0 to slightly higher than the power frequency. The attenuation time constant typically varies from 0.6 ms to 600 ms.

In both the over-damping and under-damping states, the transient zero-sequence current of a healthy feeder is approximately orthogonal to the transient zero-sequence voltage of the bus, and the polarity of the current projection with respect to
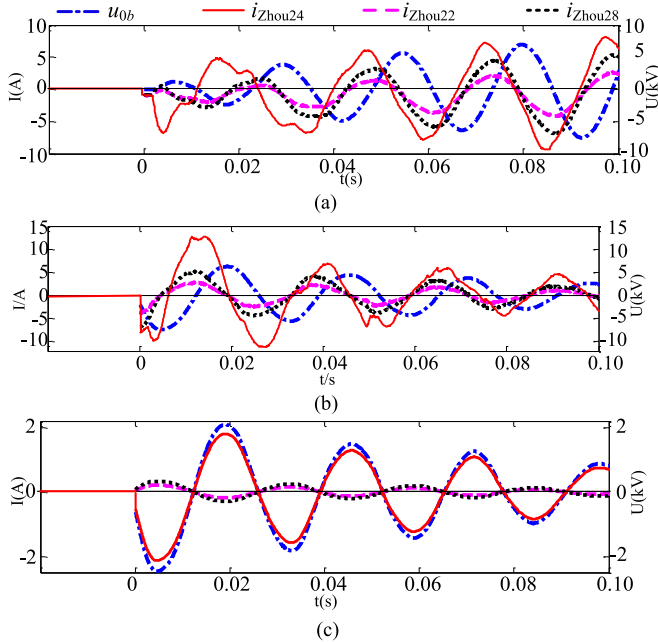
Fig. 11.   Waveforms of the field data corresponding to the under-damping state: (a) Zero-sequence component. (b) Transient component. (c) Projection component.

transient voltage is negative. The transient current of the faulty feeder consists of the transient current at the fault point and the transient capacitance ground current; the former is directly proportional (scale factor is the reciprocal of the fault resistance) to the magnitude of the transient voltage of the bus. The polarity of the projection current with respect to the transient voltage is positive, and the magnitude is larger than those of the healthy feeders.

The faulty feeder can be identified by comparing the magnitude and polarity of the transient current projection component for each feeder. The feeder with the reverse polarity of a transient current projection component among at least 3 feeders with the highest projection current is the faulty feeder. If the polarity of all the projection currents is the same, it is a bus fault. The transient analysis and transient faulty feeder identification method is verified by digital simulation and field data.

This paper established a novel faulty feeder identification method of HIF using parallel resonance electrical parameters between the Petersen coil and capacitance to ground. This method is different from the identification method of low-resistance earth faults based on the series resonance electrical parameter between the line inductance and system capacitance to ground that ignores the effect of the Petersen coil.

REFERENCES

[1] M. Aucoin, "Status of high impedance fault detection," *IEEE Trans. Power App. Syst.*, vol. PER-5, no. 3, pp. 39–40, Mar. 1985.

[2] D. Griffel and Y. Harmmand, "A new deal for safety and quality on MV networks," *IEEE Trans. Power Del.*, vol. 12, no. 4, pp. 1428–1433, Oct. 1997.

[3] Detection of downed conductors on utility distribution systems, IEEE PES Tutorial Course 90EH0310-3-PWR, 1989.

[4] B. D. Russell and C. L. Benner, "Arcing fault detection for distribution feeders: Security assessment in long term field trials," *IEEE Trans. Power Del.*, vol. 10, no. 2, pp. 676–683, Apr. 1995.

[5] B. D. Russell, B. M. Aucoin, and L. C. Benner, "Randomness fault detection system," U.S. Patent 5 485 093, Jan. 16, 1996.

[6] K. Y. Lien, S. L. Chen, C. J. Liao, and T. Y. Guo, "Energy variance criterion and threshold tuning scheme for high impedance fault detection," *IEEE Trans. Power Del.*, vol. 14, no. 3, pp. 810–817, Jul. 1999.

[7] F. B. Costa, B. A. Souza, N. S. D. Brito, J. A. C. B. Silva, and W. C. Santos, "Real-time detection of transients induced by high-impedance faults based on the boundary wavelet transform," *IEEE Trans. Ind. Appl.*, vol. 51, no. 6, pp. 5312–5323, May 2015.

[8] D. I. Jeerings and J. R. Linders, "Unique aspects of distribution system harmonics due to high impedance ground faults," *IEEE Trans. Power Del.*, vol. 5, no. 2, pp. 1086–1094, Apr. 1990.

[9] A. A. Girgis, W. Chang, and E. B. Makram, "Analysis of high-impedance fault generated signals using a Kalman filtering approach," *IEEE Trans. Power Del.*, vol. 5, no. 4, pp. 1714–1724, Oct. 1990.

[10] A. R. Sedighi, M. R. Haghifam, O. P. Malik, and M. H. Ghassemian, "High impedance fault detection based on wavelet transform and statistical pattern recognition," *IEEE Trans. Power Del.*, vol. 20, no. 4, pp. 2414–2421, Oct. 2005.

[11] M. Michalik, W. Rebizant, M. Lukowicz, S. J. Lee, and S. H. Kang, "High-impedance fault detection in distribution networks with use of wavelet-based algorithm," *IEEE Trans. Power Del.*, vol. 21, no. 4, pp. 1793–1802, Oct. 2006.

[12] J. R. Macedo, J. W. Resende, and C. A. Bissochi, Jr., "Proposition of an interharmonic-based methodology for high-impedance fault detection in distribution systems," *IET Gener., Transm. Distrib.*, vol. 9, no. 16, pp. 2593–2601, Mar. 2015.

[13] S. J. Huang and C. T. Hsieh, "High-impedance fault detection utilizing a Morlet wavelet transform approach," *IEEE Trans. Power Del.*, vol. 14, no. 4, pp. 1401–1410, Oct. 1999.

[14] H. Ma, X. Zeng, Y. Wang, and Z. Li, "Grounding fault protection with fault resistance measuring for ineffectively earthed power systems," in *Proc. IEEE/PES Transm. Distrib. Conf. Exhib.*, Aug. 2005, pp. 1–3.

[15] T. Welfonder, V. Leitloff, R. Fenillet, and S. Vitet, "Location strategies and evaluation of detection algorithms for earth faults in compensated MV distribution systems," *IEEE Trans. Power Del.*, vol. 15, no. 4, pp. 1121–1128, Oct. 2000.

[16] G. Druml, W. Klein, and O. Seifert, "New adaptive algorithm for detecting low- and high ohmic faults in meshed networks," in *Proc. 2009 CIRED Int. Conf. Exhib. Electr. Distrib.*, vol. 3, paper no. 631.

[17] G. Druml, A. Kugi, and O. Seifert, "A new directional transient relay for high ohmic earth faults," in *Proc. 2003 CIRED Int. Conf. Exhib. Electr. Distrib.*, vol.3, paper no. 350.

[18] Y. D. Xue, J. Li, and B. Y. Xu, "Transient equivalent circuit and transient analysis of single-phase earth fault in arc suppression coil grounded system," *Proc. CESS*, vol. 35, no. 22, pp. 5703–5714, Nov. 2015.

[19] B. Y. Xu, Y. D. Xue, J. Li, and Y. Chen, "Single phase fault detection technique based on transient current and its application in non-solid grounded network," in *Proc. 7th Int. Conf. Develop. Power Syst. Protection*, 2001, pp. 141–144.

[20] O. Chaari, S. P. Bastard, and M. Meunier, "Prony's method: An efficient tool for the analysis of earth fault currents in Petersen-coil-protected networks," *IEEE Trans. Power Del.*, vol. 10, no. 3, pp. 1234–1241, Jul. 1995.

Yongduan Xue (M'13) received the B.S., M.S., and Ph.D. degrees from Xi'an Jiaotong University, Xi'an, China, in 1992, 1997, and 2003, respectively. He is currently a Professor with the College of Information and Control Engineer, China University of Petroleum, Qingdao, China. His research interests include neutral grounding and single line-to-ground fault self-healing technology.

Xiaoru Chen was born in 1990. She received the bachelor's degree in electrical engineering and automation from China University of Petroleum, Qingdao, China, in 2014, where she is currently working toward the master's degree in electrical engineering. Her research interest focuses on ineffectively grounded system fault detection.

Bingyin Xu (M'95) received the B.S. and M.S. degrees in electrical engineering from Shandong University, Jinan, China, in 1982 and 1987, respectively, and the Ph.D. degree in electrical engineering from Xi'an Jiaotong University, Xi'an, China, and City University London, London, U.K., by joint training in 1991. He is currently a Professor with the College of Electrical and Electronic Engineering, Shandong University of Technology, Zibo, China. His research interests include distribution automation, fault location and monitoring of power networks, and smart grids.

Huamao Song was born in 1988. He received the bachelor's degree in electrical engineering and automation from China University of Petroleum, Qingdao, China, in 2012, where he is currently working toward the master's degree in electrical engineering. His research interest focuses on ineffectively grounded system fault detection.